INCORPORATING LONG-PERIOD (T>1 S) EARTHQUAKE GROUND MOTIONS FROM 3-D SIMULATIONS IN THE U.S. NATIONAL SEISMIC HAZARD MODEL

M. P. Moschetti[1], N. Luco[2], A. S. Baltay[3], O. S. Boyd[4], A. D. Frankel[5], R. Graves[6], M. D. Petersen[7], E. M. Thompson[8], T. H. Jordan[9], S. Callaghan[10], C. Goulet[11], K. Milner[12], P. Maechling[13]

[1] *Research geophysicist, U.S. Geological Survey, mmoschetti@usgs.gov*
[2] *Research structural engineer, US Geological Survey, nluco@usgs.gov*
[3] *Research geophysicist, U.S. Geological Survey, abaltay@usgs.gov*
[4] *Research geophysicist, U.S. Geological Survey, olboyd@usgs.gov*
[5] *Research geophysicist, U.S. Geological Survey, afrankel@usgs.gov*
[6] *Research geophysicist, U.S. Geological Survey, rwgraves@usgs.gov*
[7] *Supervisory research geophysicist, U.S. Geological Survey, mpetersen@usgs.gov*
[8] *Research geophysicist, U.S. Geological Survey, emthompson@usgs.gov*
[9] *Professor, University of Southern California and Director, Southern California Earthquake Center, tjordan@usc.edu*
[10] *Research programmer, Southern California Earthquake Center, scottcal@usc.edu*
[11] *Executive science director for special projects, Southern California Earthquake Center, cgoulet@usc.edu*
[12] *Research programmer, Southern California Earthquake Center, kmilner@usc.edu*
[13] *IT Architect, Southern California Earthquake Center, maechlin@usc.edu*

Abstract

The increasing accuracy of 3-D earthquake ground motion simulations and demand for long-period (T>1 s) probabilistic ground motions motivate the investigation of a potential method for incorporating simulated ground motions into the U.S. National Seismic Hazard Model. We present preliminary sensitivity results from an amplification-based approach to incorporating simulated ground motions into PSHA. Computations employ simulated ground motions from the Southern California Earthquake Center (SCEC) CyberShake Study 15.4. We outline a method for computing amplified ground motions and for their incorporation in probabilistic seismic hazard analysis. Empirical amplification factors from the analysis of small- to moderate-magnitude earthquakes are employed to identify CyberShake locations where the earthquake ground motions are well characterized by the ground motion prediction equations. Examining ruptures from a single seismic source from the Uniform California Earthquake Rupture Forecast, version 2, we identify a strong dependence of the amplified ground motions to the reference site and rupture realization. These preliminary results prepare the way for improved ground motion characterization at sites where sedimentary basin and finite-fault effects control the strong ground motions.

Keywords: Probabilistic seismic hazard analysis (PSHA); ground motion simulations; ground motion characterization

1. Introduction

The current state-of-practice for characterizing earthquake ground-shaking in probabilistic seismic-hazard analyses (PSHA) is the use of ground motion prediction equations (GMPEs) that describe ground motion excitation and attenuation. While modern GMPEs are developed by building models to account for the controlling physical phenomena and regressing the models to recorded motions ([1–3]), it is widely recognized that region-specific site and source effects may not be properly accounted for in GMPEs.

The effects of 3-D geologic structures—particularly sedimentary basins—and finite-source effects on earthquake ground motions are examples of site and source effects that are known to produce anomalous ground motions. Sedimentary basins have been demonstrated to cause many complicating effects to seismic wave propagation, including constructive wave-wave interference, amplified surface waves, and focusing ([4–7]). Finite-source effects arise from the spatiotemporal evolution of the earthquake rupture, for which radiated seismic waves from different parts of the fault may interact ([8]). Rupture directivity is perhaps the best-recognized finite-source effect, in which seismic waves radiated along the propagation path of the earthquake rupture constructively interfere, producing large ground motions. Earthquake ground motion modeling employing 3-D elastic wave propagation and finite-source models have succeeded in reproducing these important effects for ground motion characterization. ([9]).

There is growing interest within the seismic-hazard community in the use of earthquake simulations for characterizing ground motions, particularly in areas where ground motion prediction is complicated by the effects from 3-D geologic structures. For earthquakes occurring in the western U.S., ground motion characterization (GMC) of the U.S. national seismic hazard model has historically been provided by a suite of empirically based GMPEs ([10–12]). The GMPEs include average effects of deep sedimentary basins and finite-fault effects, such as directivity because recordings containing these features are included in the underlying database ([13]). However, even for regions with many ground motion recordings—such as the Los Angeles metropolitan area—future ground motions are likely to be far more complicated than what can currently be predicted by GMPEs ([14, 15]).

Within the U.S., ground motions from 3-D simulations form the basis for GMC in a few regional seismic hazard analyses, commonly referred to as "urban seismic hazard maps." Frankel et al. ([16]) developed seismic hazard maps for the Seattle region from 3-D simulations of earthquakes on crustal faults and within the Cascadia subduction zone, to account for the effects of the deep sediments and unique geometry of the Seattle basin and for rupture directivity. They found strong amplification of earthquake ground motions caused by focusing and surface wave generation within the Seattle basin compared to the GMPE-predicted ground motions.

More recently, the Southern California Earthquake Center (SCEC) CyberShake project has computed long-period (T≥1 s) earthquake ground motions from all Uniform California Earthquake Rupture Forecast, version 2 (UCERF2) ([17]) fault ruptures in the Los Angeles, California region ([18]). The CyberShake project is currently extending the simulations to higher frequencies and to the set of fault ruptures from UCERF3 mm([19, 20]). The CyberShake project introduced two novel methodologies for computing seismic hazard from 3-D simulations. First, the ground motion simulations are computed from a database of strain Green tensors, which exploit the reciprocity of elastic wave propagation in order to greatly reduce the requisite number of calculations of 3-D wave propagation ([21, 22]). Second, the conditional probability of exceedance curves are empirically constructed from the suite of ground motions corresponding to the numerous realizations of the slip distribution and hypocenter location for each seismic source. In this way, the CyberShake model directly employs non-ergodic ground motion distributions at all sites.

In this paper, we present preliminary results from one method for incorporating long-period (T≥1 s) ground motions from 3-D simulations into the U.S. national seismic hazard model using simulated ground motions from the CyberShake seismic hazard model. We first outline a method for introducing the average ground motion features from the simulations into the probabilistic seismic hazard calculation through the use of amplification factors. We then compute ground motion amplifications from the 3-D simulations, examine the

2

sensitivity of the calculation to the reference site conditions and compute the residuals between the amplified ground motions and best-available GMPEs.
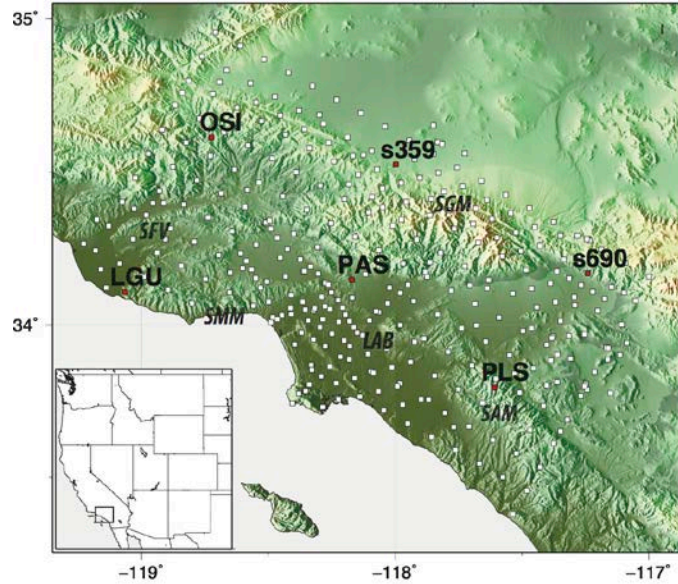

Figure 1: CyberShake locations and reference, rock sites identified from empirical amplification factors. All CyberShake locations are depicted by white squares. Reference sites (OSI, LGU, s359, PAS, PLS, s690) are depicted by red circles and labeled by their CyberShake names. Physiographic regions are labeled with boldface, italic text: Santa Ana Mountains (SAM), San Fernando Valley (SFV), San Gabriel Mountains (SGM), Santa Monica Mountains (SMM), Los Angeles Basin (LAB). Inset map provides regional context.

2. Conditional probabilities of exceedance from simulated ground motions

2.1 Framework for incorporating modified-means into PSHA

Probabilistic seismic hazard analysis (PSHA) provides the rate at which a specified ground motion is exceeded ("rate of exceedance") ([23–25]) and is widely applied in engineering design. In this context, we use the term "ground motion" to refer to true measures of earthquake-induced ground-shaking (e.g., peak ground acceleration, peak ground velocity) and to maximum response spectral parameters (e.g., response spectral accelerations). In the U.S., the NSHM—and its derivative seismic hazard maps—are obtained from a national-scale PSHA ([10, 11]) and form the basis for the seismic provisions of the building codes ([26]).

At a particular location, the rates of exceedance are typically computed from the discretized form of the hazard integral and may be expressed as (e.g., Baker, 2008):

$$\lambda(Y > y) = \sum_{i=1}^{n} \lambda(M_i > m_{min}) \sum_{j=1}^{n_M} \sum_{k=1}^{n_R} P(Y > y|m_j, r_k) P(M_i = m_j) P(R_i = r_k) \tag{1}$$

Where $\lambda(Y > y)$ and $\lambda(M_i > m_{min})$ are the rate of exceeding the ground motion y and the rate of earthquakes with magnitudes M_i greater than m_{min}, respectively. $P(M_i = m_j)$ and $P(R_i = r_k)$ are the probabilities characterizing earthquake magnitudes m_j and source-to-site distances r_k. Most importantly, for this paper, is the probability of exceedance that the ground motion exceeds y, conditioned on the occurrence of an earthquake with magnitude m_j, at the location r_k, which we refer to as the "conditional probabilities of exceedance," $P(Y > y|m_j, r_k)$.

3

PSHA typically assumes the use of a log-normal distribution of ground motions, permitting calculation of the conditional probabilities of exceedance from the mean $\mu(m_j, r_k)$ and standard deviation (sigma) $\sigma(m_j, r_k)$ of the predicted, logarithmized distribution:

$$P(Y > y|m_j, r_k) = 1 - \Phi\left(\frac{\ln(y) - \mu(m_j, r_k)}{\sigma(m_j, r_k)}\right) \tag{2}$$

Ground motion means and sigmas for the NSHM are currently obtained from suites of ground motion prediction equations (GMPEs) appropriate for the regional seismotectonics. For example, the 2014 NSHM used five GMPEs to characterize ground motions from shallow crustal earthquakes in the western U.S. ([27–31]).

Our focus is on exploring one method for modifying the mean (logarithmized) ground motions $\mu(m_j, r_k)$ employed in calculating the conditional probabilities of exceedance:

$$\mu_{mod}(m_j, r_k) = \mu(m_j, r_k) + \delta(m_j, r_k) \tag{3}$$

Identifying such amplification factors $\delta(m_j, r_k)$—which may vary with source and site—may be implemented for PSHA in a straightforward manner to provide the exceedance probability incorporating the average (basin and finite-fault) features of 3-D simulations, $P_{sim}(Y > y|m_j, r_k)$:

$$P_{sim}(Y > y|m_j, r_k) = 1 - \Phi\left(\frac{\ln(y) - \mu(m_j, r_k) - \delta(m_j, r_k)}{\sigma(m_j, r_k)}\right) \tag{4}$$

The goal of this work is the incorporation of regionally appropriate basin amplification and finite fault effects into seismic hazard analyses. Because these effects are incorporated in GMPEs in an average manner, but strongly depend on local basin geometry and fault orientations, this effort may greatly improve seismic hazard characterizations. This sensitivity study of amplification factors was recommended by the U.S. Geological Survey Working Group on Urban Seismic Hazard Models. The recommendation was based on the viewpoint that the mean values from the simulations may be more robust than the full ground motion distributions, which require knowledge and proper characterization of the underlying source rupture parameters. However, we recognize that alternative methods exist for incorporating the ground motions from 3-D simulations into the NSHM and PSHA, in general (e.g., [32]). Unlike CyberShake, this approach does not modify the standard deviations of the ground motion distributions, and therefore, cannot reduce the uncertainty contribution from the ground motion distribution ([33]).

We explore spatially varying ground motion amplifications relative to the GMPE-predicted ground motions by analyzing sets of ground motions from individual seismic sources. For comparison, the CyberShake project employs a fundamentally different approach to computing the conditional probabilities of exceedance by constructing an empirical conditional probability curve from the suite of ground motion simulations.

2.2 Cybershake Ground motion simulations

The sensitivity calculations use the ground motions from CyberShake Study 15.4. We briefly summarize details of the simulations here. Full details about the CyberShake methodology and simulations can be found in Graves et al. ([18]) and at the CyberShake Project website[1]. CyberShake simulations comprise the ~7,000 seismic sources from the Uniform California Earthquake Rupture Forecast, Version 2 ([17]) that affect sites in the CyberShake region, with variations in the slip distribution and hypocenter location for each source. We use the term "seismic source" in the context of seismic source characterization for PSHA—the magnitude, location, and recurrence of one event (e.g., [11, 34, 35]). We refer to each realization of slip distribution and hypocenter location as one rupture model for the particular seismic source. The ground motion simulations employ 3-D seismic velocity models of southern California ([36, 37]) that have been subjected to various updates and testing with small- to moderate-sized local earthquakes ([38–40]). Anelastic seismic wave propagation is computed with finite-difference code, AWP-ODC ([41, 42]). The CyberShake workflow outputs ground motion time series at

---

[1] https://scec.usc.edu/scecpedia/CyberShake, last accessed May 4, 2016

each site, for all seismic sources and slip-hypocenter realizations, with a maximum frequency of 1 Hz. Our analysis focuses on response spectral accelerations (2, 3, 5 s periods) computed from the geometric mean of the horizontal-component time series.

3. Methodology for computing amplified ground motions

We follow the approach developed by Frankel et al. ([16]) to compute the amplified ground motions from the CyberShake simulations. For each CyberShake location, we compute the amplification of 5-percent-damped pseudo-spectral acceleration SA for a particular site s_i, source e_j and rupture h_k relative to the ground motions at a reference site s_{ref}:

$$A_{ref}(s_i, e_j, h_k) = \frac{SA(s_i, e_j, h_k)}{SA(s_{ref}, e_j, h_k)} \tag{5}$$

Amplified ground motions from a specified reference site $SA_{amp,ref}$ are then computed from the GMPE-predicted ground motions, with Vs30=760 m/s, $SA_{GMPE}^{Vs30=760}$ as:

$$SA_{amp,ref}(s_i, e_j, h_k, r_{ref}) = A_{ref}(s_i, e_j, h_k) SA_{GMPE}^{Vs30=760}(s_{ref}, e_j) \tag{6}$$

For the case of multiple rupture models—such as the multiple (N) realizations of slip distributions and hypocenter locations of CyberShake—and multiple (N_{ref}) reference sites with relative weightings w_{ref}, the amplified ground motion computation generalizes to:

$$SA_{amp}(s_i, e_j) = \sum_{ref=1}^{N_{ref}} w_{ref} \left(\frac{SA_{GMPE}^{Vs30=760}(s_{ref}, e_j)}{N} \sum_{k=1}^{N} A_{ref}(s_i, e_j, h_k) \right) \tag{7}$$
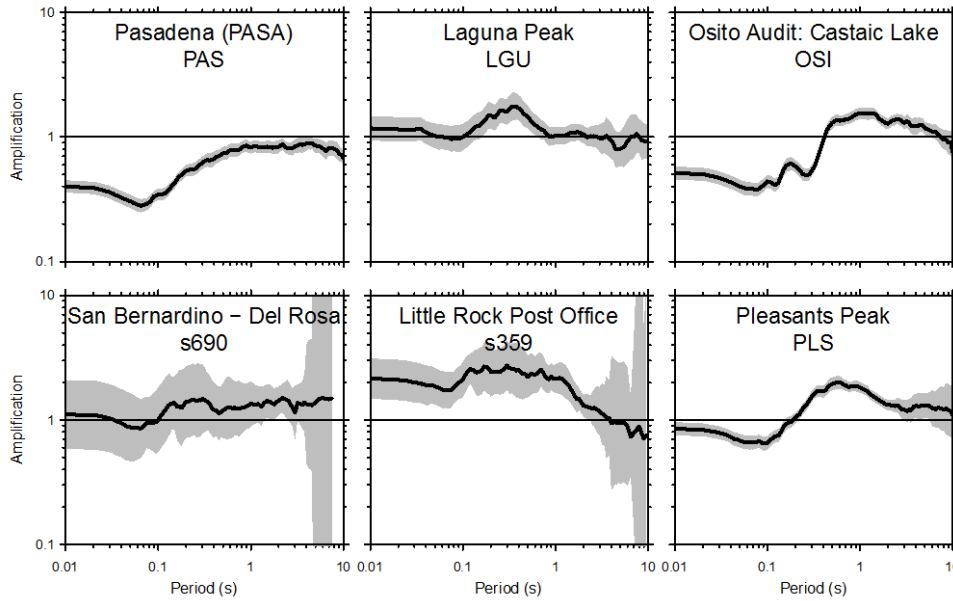

Figure 2: Empirical amplification factors near six CyberShake locations (PAS, LGU, OSI, s690, s359, PLS), where the empirical ground motion response at 2, 3 and 5 s oscillator periods is similar ($\pm 60\%$) to the GMPE-predicted ground motions. Black lines depict the mean ground motion amplifications, with the gray envelope showing the standard error.

This approach for computing amplified ground motions captures the average amplifications caused by sedimentary basins and finite source effects, while also requiring that the simulated ground motions match the

ground motions from the GMPEs for reference rock sites. Agreement between the simulated and GMPE-predicted motions at rock sites is a critical requirement for the national-scale PSHA of the NSHM, where uniform conditions (Vs30=760 m/s) prevail ([10],[11]), and we wish to avoid step functions in predicted ground motions, especially for rock sites, where the large database of ground motions gives us good confidence in the empirical results ([13]).

3.1 Identifying reference, rock sites

A critical issue for these computations is the identification of CyberShake locations where the ground motions are well characterized by the GMPEs. We employed empirical amplification factors (EAFs) ([43]) computed for seismometers in southern California to identify stations where the recorded ground motions are within a factor of 1.6 of the GMPE-predicted ground motions at oscillator periods of 2, 3 and 5 s (Figure 1). We observed significant variability in the shorter period (T<2 s) EAFs for the selected sites that largely reflect the varying nature of the shallow subsurface; however, these responses are of no consequence to the long-period ground motions of interest. Six reference sites were identified as being located within 1 km of a seismic station expressing acceptable long-period empirical amplification with respect to the GMPEs. Ground motions at these reference sites behave similarly to GMPE-predicted (Vs30=760 m/s) ground motions.
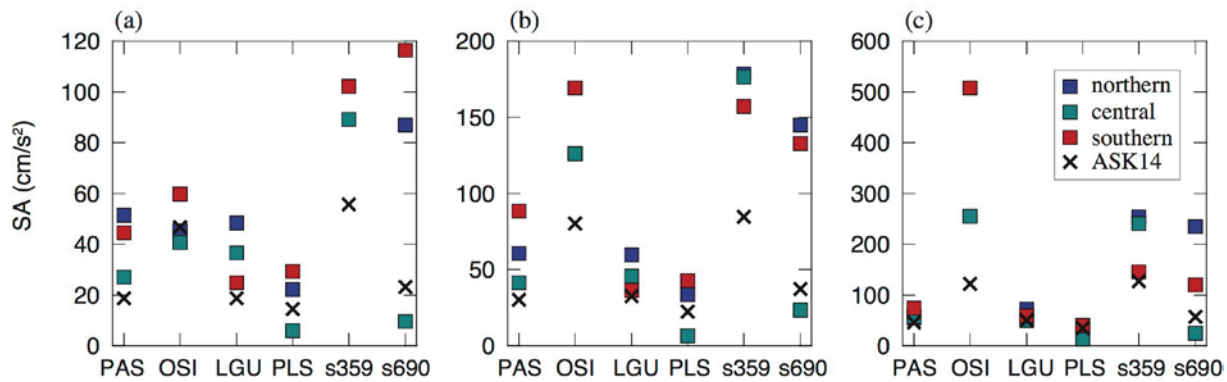

Figure 3. Response spectral accelerations from ruptures scenarios of M7.9 southern San Andreas earthquakes and from the Abrahamson et al. (2014) [27] (ASK14) GMPE for (a) 5 s, (b) 3 s and (c) 2 s periods are depicted at the six reference rock-sites. The legend indicates hypocenter location.

4. Amplified ground motions from representative sources

We computed amplified ground motions from one UCERF2 seismic source to begin to examine the sensitivity to underlying rupture parameters and reference sites. The seismic source for this sensitivity study is the southern San Andreas (CH+CC+BB+NM+SM) M7.85 (source 64, rupture 3) with hypocenters located at northern, central and southern positions (variations 67, 199, 223), representing three rupture models as defined earlier. All ground motions were taken from the calculations of SCEC CyberShake Study 15.4.

Simulated ground motions at the reference rock sites exhibit variable sensitivity to the rupture scenarios (Fig. 3). Although ground motion variability at many sites is relatively small (e.g., PAS, 5 s), some stations exhibit significant variability. For example, site s690 at 5 s period, records ground motions ranging 9.6–116.5 cm/s^2 for the three rupture models. Presumably, the large variations in ground motion are caused by directivity and the distance and orientation of controlling slip patches from the rupture scenarios. Fig. 3 also includes the predicted ground motions from the Abrahamson et al. ([27]) GMPE. The apparent discrepancy between the simulated and GMPE-predicted ground motions at some reference sites may be caused by the incomplete rupture set of this sensitivity test, strong and persistent finite-fault effects, or errors in the empirically based GMPE. While our approach enforces the empirically based ground motions at these sites (Eq. 6), investigation of these discrepancies and their effects on the amplified ground motions is warranted.

Using all three selected ruptures, we compute amplified ground motions for each reference site (Eq. 6). Unsurprisingly, and not presented here, we observed a strong dependence of the amplified ground motions to the rupture realization because of finite-fault effects, most notably source directivity. Examples of the amplified ground motions from the six reference sites, at 5 s period, are depicted in Fig. 4. The spatial patterns of the reference site amplified ground motions show high similarity. However, the absolute ground motions vary by up to a factor of about 2. The spatial patterns from the 3 and 2 s period amplifications are similar, and the differences among the reference sites are less than for the 5 s result.
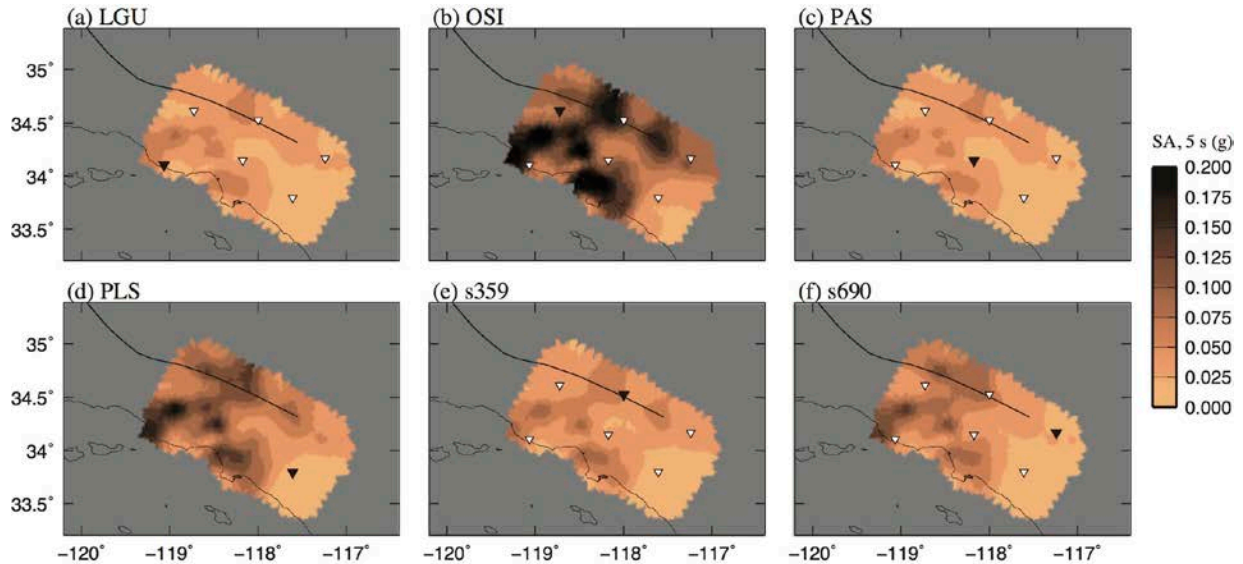

Figure 4. Amplified ground motions, 5 s spectral accelerations (Eq. 6), for the six reference rock sites of the study (LGU, OSI, PAS, PLS, s359, s690).
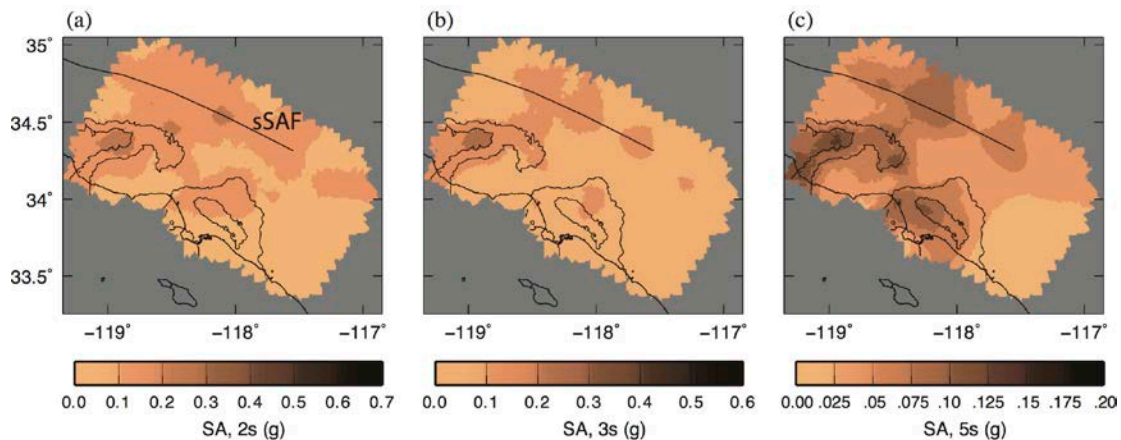

Figure 5. Amplified ground motions for source 64, rupture, southern San Andreas (sSAF) seismic source. Panels depict spectral accelerations at oscillator periods of (a) 2 s, (b) 3 s and (c) 5 s. Panels include 2- and 4-km contours of Z2.5 depths. The fault trace is plotted in all panels and labeled in panel (a).

Although all reference sites were selected to exhibit ground motion response that agreed with Vs30=760 m/s GMPE predictions, the empirical amplifications were derived for small- to moderate-sized earthquakes and did not account for strong rupture directivity. In addition, our criterion for identifying reference rock sites

permits site-to-site amplification-discrepancies of about a factor of 3. We interpret the reference site dependence to result from a combination of directivity effects and minor variations in site response. We employ equal weighting of all reference sites (Eq. 7) because we aim to capture average basin and finite-fault effects, and we judge that use of increasing numbers of reference sites stabilizes these results.

The final amplified ground motions (Eq. 7) computed with employing equal weights for all reference-site-amplifications are depicted in Fig. 5. The spatial patterns of the amplified ground motions are similar at all periods, with ground motion levels decreasing with increasing period. Amplified ground motions are high in the near-source region and at sites overlying the sedimentary basins.

4.2 Residuals between the amplified ground motions and GMPEs

We compute the ground motion residual parameter ε to identify differences between the amplified ground motions (Eq. 7) and the NGA-W2 GMPEs. The ε values highlight differences between the adjusted, simulated ground motions, which are constrained to match the GMPE predictions at the reference sites, and the predictions from the GMPEs:

$$\varepsilon(s_i, e_j) = \frac{\ln SA_{amp}(s_i,e_j) - \ln SA_{GMPE}^{Vs30,Z1,Z2.5}(s_i,e_j)}{\sigma_{GMPE,ln}(s_i,e_j)} \quad (8)$$

Examples of the ε values from the use of the ASK14 GMPE are presented in Fig. 6. The GMPE-predicted ground motions employ variable Vs30 and basin depths (Z1, Z2.5) to provide the best-possible empirically derived characterization of the ground motion. We did not implement empirical adjustments for directivity (e.g., [44]), which may reduce ground motion discrepancies—and result in smaller ε values—between the GMPEs and the amplified ground motions in those areas affected by rupture directivity.
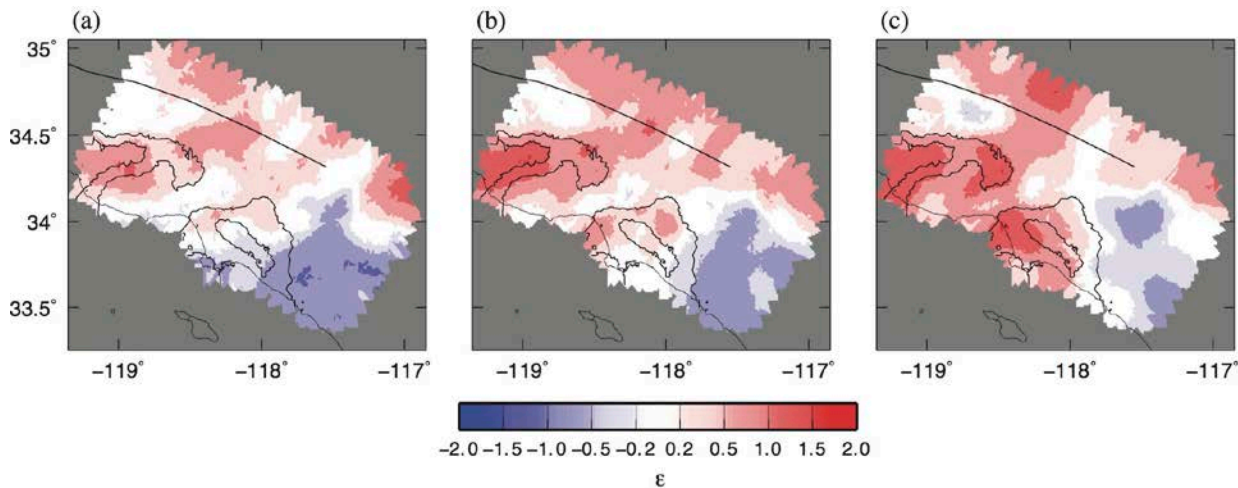

Figure 6. Residuals (ε) for amplified ground motions from source 64, southern San Andreas Fault, computed with the ASK14-predicted ground motions. Panels depict ☐ values for and (c) 5 s.

Ground motion residuals exhibit strong correspondence with geologic structures and the seismic source, indicating differential source and basin effects from the 3-D simulations compared to the empirically based GMPEs. Large, positive ground motion residuals are associated with the deep sedimentary basins of the Los Angeles region. The amplified ground motions indicate that rupture of the southern San Andreas Fault strongly amplifies ground motions in the deep basins of the Los Angeles metropolitan region. Amplifications are particularly pronounced through the San Fernando Valley and increase with increasing oscillator period. These calculations reproduce earlier numerical and semi-empirical observations of the strong excitation of seismic waves within the Los Angeles sedimentary basins from earthquakes on the San Andreas Fault and lead to greatly

increased long-period ground motions, relative to the predictions from GMPEs ([15],[45],[32]). For the 2 and 3 s results, the ground motion residuals in the Santa Monica Mountains are close to zero, indicating a relative agreement between the simulated and GMPE-predicted ground motions; at 5 s, the ground motions from the 3-D simulation are slightly elevated with respect to the GMPE-predicted ground motions.
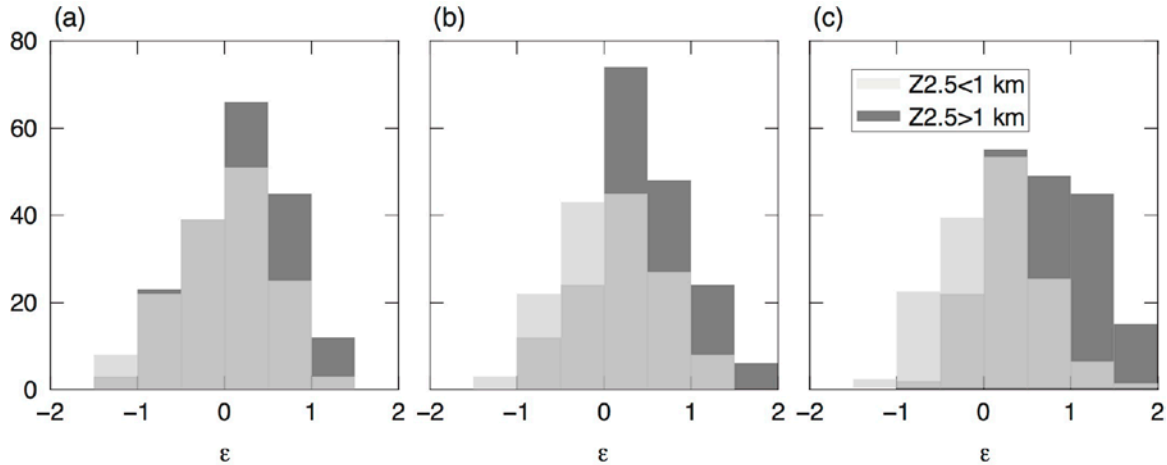

Figure 7. Histograms of ε for CyberShake locations at shallow ($Z2.5 < 1\ km$) and deep ($Z2.5 \geq 1\ km$) basin sites for periods of (a) 2 s, (b) 3 s and (c) 5 s. Mean values of the distributions are presented in Table 1.

Histograms of the ε values for shallow ($Z2.5 < 1\ km$) and deep ($Z2.5 \geq 1\ km$) basin sites further indicate the greater ground motions resulting from the simulations compared to the empirical GMPEs. Histograms from the shallow sites are generally centered about $\varepsilon = 0$, while the histograms from the deeper sites indicate most ε values are positive. Mean ε values ($\bar{\varepsilon}$) are tabulated in Table 1. For all periods, the ground motion residuals for the shallow basin sites are small ($|\bar{\varepsilon}| < 0.1$), indicating a good general agreement between the GMPE-predicted and simulated ground motions. For the deeper basin sites ($Z2.5 \geq 1\ km$), $\bar{\varepsilon}$ values range 0.18–0.65 and increase with oscillator period.

Table 1: Mean $\bar{\varepsilon}$ values from shallow ($Z2.5 < 1\ km$) and deep ($Z2.5 \geq 1\ km$) sedimentary basin sites.

Period (s)	$\bar{\varepsilon}, Z2.5 < 1\ km$	$\bar{\varepsilon}, Z2.5 \geq 1\ km$
2	-0.01	0.18
3	0.08	0.42
5	0.08	0.65

5. Conclusions

Following the amplification method applied in the Seattle urban seismic hazard model, we outline a method for incorporating simulated ground motions into the U.S. National Seismic Hazard Model by modifying the mean of the probability density function describing the ground motion distribution. The method captures important basin and finite-fault effects, which are strongly influenced by the basin and fault geometries for the Los Angeles metropolitan region, but also ensures agreement between the simulated ground motions and the empirically derived ground motion prediction equations at reference rock sites. This approach has the benefit of requiring that the amplified ground motions from the simulations match the empirically predicted ground motions.

We perform preliminary sensitivity tests of the amplification computation using ground motions from the CyberShake project. We focused on variations of the ground motions from a M7.9 earthquake on the southern

San Andreas Fault, with hypocenter locations at the northern, central and southern parts of the fault. Reference rock-site locations were identified from the set of CyberShake locations by examining empirical amplification factors from small- to moderate-sized earthquakes. Despite the fact that the empirical amplifications of the reference sites exhibited good agreement with GMPE-predicted ground motions, we find significant variation in the amplified ground motions resulting from the six reference sites. The weighted, amplified ground motions show good general agreement with empirically predicted ground motions for sites where the sediment depths are shallow ($Z2.5 < 1\ km$). At sites overlying deeper sediments ($Z2.5 \geq 1\ km$), the amplified ground motions are significantly greater, on average, than what is predicted by the GMPEs, and the discrepancy increases with increasing oscillator period. This observation is consistent with previous analyses and suggests that the simulated ground motions—and the resulting amplified ground motions—may better predict the strong ground shaking that may be expected at basin sites in the Los Angeles region for future earthquakes.

6. Acknowledgements

7. References

[1] Abrahamson NA, Silva WJ (1997): Empirical response spectral attenuation relations for shallow crustal earthquakes. *Seismol. Res. Lett.*, **68**(1), 94–127.

[2] Douglas J (2003): Earthquake ground motion estimation using strong-motion records: a review of equations for the estimation of peak ground acceleration and response spectral ordinates. *Earth-Sci. Rev.*, **61**(1), 43–104.

[3] Akkar S, Bommer JJ (2007): Empirical prediction equations for peak ground velocity derived from strong-motion records from Europe and the Middle East. *Bull. Seismol. Soc. Am.*, **97**(2), 511–530.

[4] Kawase H (1996): The cause of the damage belt in Kobe:"The basin-edge effect," constructive interference of the direct S-wave with the basin-induced diffracted/Rayleigh waves. *Seismol. Res. Lett.*, **67**(5), 25–34.

[5] Hartzell S, Cranswick E, Frankel A, Carver D, Meremonte M (1997): Variability of site response in the Los Angeles urban area. *Bull. Seismol. Soc. Am.*, **87**(6), 1377–1400.

[6] Frankel A, Carver D, Cranswick E, Meremonte M, Bice T, Overturf D (1999): Site response for Seattle and source parameters of earthquakes in the Puget Sound region. *Bull. Seismol. Soc. Am.*, **89**(2), 468–483.

[7] Graves RW, Pitarka A, Somerville PG (1998): Ground-motion amplification in the Santa Monica area: Effects of shallow basin-edge structure. *Bull. Seismol. Soc. Am.*, **88**(5), 1224–1242.

[8] Archuleta RJ, Hartzell SH (1981): Effects of fault finiteness on near-source ground motion. *Bull. Seismol. Soc. Am.*, **71**(4), 939–957.

[9] Frankel A, Stephenson W, Carver D (2009): Sedimentary basin effects in Seattle, Washington: Ground-motion observations and 3D simulations. *Bull. Seismol. Soc. Am.*, **99**(3), 1579–1611.

[10] Frankel AD, Mueller C, Barnhard T, Perkins D, Leyendecker E, Dickman N, Hanson S, Hopper M (1996): National seismic-hazard maps: documentation June 1996. US Geological Survey Reston, VA.

[11] Petersen MD, Moschetti MP, Powers PM, Mueller CS, Haller KM, Frankel AD, Zeng Y, Rezaeian S, Harmsen SC, Boyd OS (2015): The 2014 United States national seismic hazard model. *Earthq. Spectra*, **31**(S1), S1–S30.

[12] Rezaeian S, Petersen MD, Moschetti MP, Powers P, Harmsen SC, Frankel AD (2014): Implementation of NGA-West2 ground motion models in the 2014 US National Seismic Hazard Maps. *Earthq. Spectra*, **30**(3), 1319–1333.

[13] Ancheta TD, Darragh RB, Stewart JP, Seyhan E, Silva WJ, Chiou BS-J, Wooddell KE, Graves RW, Kottke AR, Boore DM (2014): NGA-West2 database. *Earthq. Spectra*, **30**(3), 989–1005.

[14] Olsen KB (2000): Site amplification in the Los Angeles basin from three-dimensional modeling of ground motion. *Bull. Seismol. Soc. Am.*, **90**(6B), S77–S94.

[15] Graves RW, Aagaard BT, Hudnut KW (2011): The ShakeOut earthquake source and ground motion simulations. *Earthq. Spectra*, **27**(2), 273–291.

[16] Frankel AD, Stephenson WJ, Carver DL, Williams RA, Odum JK, Rhea S (2007): Seismic hazard maps for Seattle, Washington, incorporating 3D sedimentary basin effects, nonlinear site response, and rupture directivity. Geological Survey (US).

[17] Field EH, Dawson TE, Felzer KR, Frankel AD, Gupta V, Jordan TH, Parsons T, Petersen MD, Stein RS, Weldon RJ (2009): Uniform California earthquake rupture forecast, version 2 (UCERF 2). *Bull. Seismol. Soc. Am.*, **99**(4), 2053–2107.

[18] Graves R, Jordan TH, Callaghan S, Deelman E, Field E, Juve G, Kesselman C, Maechling P, Mehta G, Milner K (2011): CyberShake: a physics-based seismic hazard model for Southern California. *Pure Appl. Geophys.*, **168**(3-4), 367–381.

[19] Callaghan S, Deelman E, Gunter D, Juve G, Maechling P, Brooks C, Vahi K, Milner K, Graves R, Field E (2010): Scaling up workflow-based applications. *J. Comput. Syst. Sci.*, **76**(6), 428–446.

[20] Field EH, Arrowsmith RJ, Biasi GP, Bird P, Dawson TE, Felzer KR, Jackson DD, Johnson KM, Jordan TH, Madden C (2014): Uniform California Earthquake Rupture Forecast, Version 3 (UCERF3)—The Time-Independent Model. *Bull. Seismol. Soc. Am.*, **104**(3), 1122–1180.

[21] Aki K, Richards PG (2002): Quantitative seismology.

[22] Zhao L, Chen P, Jordan TH (2006): Strain Green's tensors, reciprocity, and their applications to seismic source and structure studies. *Bull. Seismol. Soc. Am.*, **96**(5), 1753–1763.

[23] Cornell CA (1968): Engineering seismic risk analysis. *Bull. Seismol. Soc. Am.*, **58**(5), 1583–1606.

[24] Esteva L (1969): Seismicity prediction: a Bayesian approach. In *Proceedings of the fourth world conference on earthquake engineering*.

[25] McGuire RK (2004): Seismic hazard and risk analysis. Earthquake Engineering Research Institute.

[26] Luco N, Bachman RE, Crouse CB, Harris JR, Hooper JD, Kircher CA, Caldwell PJ, Rukstales KS (2015): Updates to building-code maps for the 2015 NEHRP recommended seismic provisions. *Earthq. Spectra*, **31**(S1), S245–S271.

[27] Abrahamson NA, Silva WJ, Kamai R (2014): Summary of the ASK14 ground motion relation for active crustal regions. *Earthq. Spectra*, **30**(3), 1025–1055.

[28] Boore DM, Stewart JP, Seyhan E, Atkinson GM (2014): NGA-West2 equations for predicting PGA, PGV, and 5% damped PSA for shallow crustal earthquakes. *Earthq. Spectra*, **30**(3), 1057–1085.

[29] Campbell KW, Bozorgnia Y (2014): NGA-West2 ground motion model for the average horizontal components of PGA, PGV, and 5% damped linear acceleration response spectra. *Earthq. Spectra*, **30**(3), 1087–1115.

[30] Chiou BS-J, Youngs RR (2014): Update of the Chiou and Youngs NGA model for the average horizontal component of peak ground motion and response spectra. *Earthq. Spectra*, **30**(3), 1117–1153.

[31] Idriss IM (2014): An NGA-West2 empirical model for estimating the horizontal spectral values generated by shallow crustal earthquakes. *Earthq. Spectra*, **30**(3), 1155–1177.

[32] Wang F, Jordan TH (2014): Comparison of probabilistic seismic-hazard models using averaging-based factorization. *Bull. Seismol. Soc. Am.*, **104**(3), 1230–1257.

[33] Jordan T (2015): How Much Can the Total Aleatory Variability of Empirical Ground Motion Prediction Equations Be Reduced Using Physics-Based Earthquake Simulations? In *2015 AGU Fall Meeting*, Agu.

[34] Frankel AD, Mueller CS, Barnhard TP, Leyendecker EV, Wesson RL, Harmsen SC, Klein FW, Perkins DM, Dickman NC, Hanson SL (2000): USGS national seismic hazard maps. *Earthq. Spectra*, **16**(1), 1–19.

[35] Moschetti MP, Powers PM, Petersen MD, Boyd OS, Chen R, Field EH, Frankel AD, Haller KM, Harmsen SC, Mueller CS (2015): Seismic source characterization for the 2014 update of the US national seismic hazard model. *Earthq. Spectra*, **31**(S1), S31–S57.

[36] Magistrale H, McLaughlin K, Day S (1996): A geology-based 3D velocity model of the Los Angeles basin sediments. *Bull. Seismol. Soc. Am.*, **86**(4), 1161–1166.

[37] Süss MP, Shaw JH (2003): P wave seismic velocity structure derived from sonic logs and industry reflection data in the Los Angeles basin, California. *J. Geophys. Res. Solid Earth*, **108**(B3).

[38] Kohler MD, Magistrale H, Clayton RW (2003): Mantle heterogeneities and the SCEC reference three-dimensional seismic velocity model version 3. *Bull. Seismol. Soc. Am.*, **93**(2), 757–774.

[39] Shaw JH, Plesch A, Tape C, Suess MP, Jordan TH, Ely G, Hauksson E, Tromp J, Tanimoto T, Graves R (2015): Unified Structural Representation of the southern California crust and upper mantle. *Earth Planet. Sci. Lett.*, **415**, 1–15.

[40] Taborda R, Azizzadeh-Roodpish S, Khoshnevis N, Cheng K (2016): Evaluation of the southern California seismic velocity models through simulation of recorded events. *Geophys. J. Int.*, **205**(3), 1342–1364.

[41] Olsen KB, Day SM, Minster JB, Cui Y, Chourasia A, Faerman M, Moore R, Maechling P, Jordan T (2006): Strong shaking in Los Angeles expected from southern San Andreas earthquake. *Geophys. Res. Lett.*, **33**(7).

[42] Cui Y, Olsen KB, Jordan TH, Lee K, Zhou J, Small P, Roten D, Ely G, Panda DK, Chourasia A (2010): Scalable earthquake simulation on petascale supercomputers. In *Proceedings of the 2010 ACM/IEEE International Conference for High Performance Computing, Networking, Storage and Analysis*, IEEE Computer Society. pp.1–20.

[43] Thompson EM, Wald DJ (2016): Uncertainty in VS30-Based Site Response. *Bull. Seismol. Soc. Am.*

[44] Spudich P, Rowshandel B, Shahi SK, Baker JW, Chiou BS-J (2014): Comparison of NGA-West2 directivity models. *Earthq. Spectra*, **30**(3), 1199–1221.

[45] Denolle MA, Dunham EM, Prieto GA, Beroza GC (2014): Strong ground motion prediction using virtual earthquakes. *Science*, **343**(6169), 399–403.